POLITECNICO DI TORINO
Repository ISTITUZIONALE

Refined beam finite elements for static and dynamic analysis of hull structures

Original
Refined beam finite elements for static and dynamic analysis of hull structures / Carrera, Erasmo; Pagani, Alfonso; Rehan, Rehan. - In: COMPUTERS & STRUCTURES. - ISSN 0045-7949. - STAMPA. - 167:(2016), pp. 37-49. [10.1016/j.compstruc.2016.01.015]

Availability:
This version is available at: 11583/2635366 since: 2016-02-25T09:12:35Z

Publisher:
Elsevier

Published
DOI:10.1016/j.compstruc.2016.01.015

Terms of use:

This article is made available under terms and conditions as specified in the corresponding bibliographic description in the repository

Publisher copyright

(Article begins on next page)

03 June 2024

Refined beam finite elements for static and dynamic analysis of hull structures

Erasmo Carrera*, Alfonso Pagani†, Rehan Jamshed‡

MUL^2 Group, Department of Mechanical and Aerospace Engineering, Politecnico di Torino
Corso Duca degli Abruzzi 24, 10129 Torino, Italy

Abstract

The accuracy and reliability of structural analyses are significantly compromised owing to the utilization of simple beam elements to model the global mechanical behaviour of ship hulls. These 1D models entail various assumptions and do not provide accurate and reliable results for hulls with complex structural details, such as cut-outs or reinforcements. The 3D FEM solutions, on the other hand, are computationally expensive. In the present study, refined 1D FE models for the analysis of simplified naval engineering structures have been developed by using the well-known Carrera Unified Formulation (CUF). According to CUF, refined kinematics beam models that go beyond classical theories (Euler, Timoshenko) can be easily developed by expressing the displacement field as an expansion in terms of generic functions, whose form and order are arbitrary. Hence, the stiffness and mass matrices are written in terms of fundamental nuclei, which are independent of the adopted class of beam theory and the FE approximation along the beam axis. As a particular class of CUF models, Lagrange polynomials have been used to formulate beam models at the component scale. According to this approach, each structural component (e.g. hull, longerons, bulkheads, and floors) can be modeled by means of the same 1D formulation. The results clearly demonstrate the enhanced capabilities of the proposed formulation, which is able to replicate solid/shell ANSYS solutions with very low computational efforts.

Keywords: Higher-order beam models; unified formulation; hull structures; component-wise.

*Professor, e-mail: erasmo.carrera@polito.it
†Research scientist, e-mail: alfonso.pagani@polito.it
‡Ph.D. student, e-mail: rehan.rehan@polito.it

1 Introduction

Ships are the largest man made structures used for transportation purposes. Owing to the growing needs, their sizes continue to grow bigger in parallel to the speed and endurance in highly dynamic environment. Ship structure designers are challenged by the need to stiffen the large ships, such as container vessels, against these dynamic loads as well as increase their capacity to carry maximum payload.

At global level, large container ships more resemble like a beam and thus are highly flexible with large amplitudes in vertical bending vibrations as compared to the others. As much as for the ship structure itself, such vibration behaviour is detrimental for various installations on board the ships that cannot withstand such large amplitudes. Thus, an accurate and reliable structural behaviour needs be predicted. The problem has been addressed by the structural analysts by employing both beam models, which are overly simple, as well as 3D solid FEM, which is computationally expensive.

The famous Euler-Bernoulli [1] and Timoshenko [2, 3] Beam Models (hereinafter referred to as EBBM and TBM, respectively) have been considerably used in the early works to model global structural behaviour of ships. According to EBBM, it is assumed that the plane cross-sections of a beam will remain plane during bending. This assumption is acceptable as long as one is interested only in vertical deflection of beam center line and is valid only for the cases of simple, solid and homogenous sections and long beams. The transverse shear stresses that become pronounced in short beams are ignored in EBBM. TBM adds one more degree of freedom to EBBM by removing the perpendicularity condition of cross section from beam axis but the plane cross sections remain plane. One of the limitations in TBM is assuming the constant shear stress distribution over beam cross-section and a correction factor is needed to be introduced to account for the homogenous stress conditions at cross-section edges. Both EBBM and TBM theories do not capture cross-section warping.

The famous British scientist Young (*Young's Modulus* named after him) employed beam theory

to find the shear stress and bending moment distributions under the distributed load and buoyancy forces. In a paper presented by John [4], a ship was considered as a beam and plate thickness was determined based on ultimate strength compared to the normal stresses. The cross-section warping of the open-sectioned ships under torsional loading was analysed by Paik et al. [5]. The first review article on hull girder strength [6], is a commendable effort citing a number of articles with hull girder modelled as beams.

The area of ship global vibration behaviour is addressed as part of the hydroelastic study of marine structures. The pioneering works of Bishop and Price [7, 8, 9] mainly focused on the surface loads and their effects on marine structures, establishing symmetric, anti-symmetric, and asymmetric two-dimensional (2D) hydroelasticity theories to determine structural behaviour, based on 2D modeling of both the ship structure and the surrounding fluid. In later decades, there has been extensive development of linear and non-linear 2D and 3D hydroelasticity theories of ships, mainly covering global load assessment and determining springing or whipping behaviour of ships and other arbitrary shaped marine structures ([10, 11, 12]. For the cases with structure in stationary waves, the approach of 3D hydroelastic analyses was simplified and was applied to various hydroelastic problems of ships and marine structures ([13, 14, 15]). These works include the analysis of stationery floating structures in waves, as product carrier [14], floating dock [15], towed jack-up [16], submerged cylinder [17], and Very Large Floating Structures (VLFSs) [18, 19, 20, 21], to the loads and safety assessment of mono-hull and multi-hull ships travelling in a seaway [22, 23]. Considerable increase in ship dimensions such as container ships and tankers has drawn interest of researchers in their hydroelasticity of springing and whipping behaviour. Malenica et al. [24] presented global hydroelastic model for ship-type bodies and validated both in frequency and time domains. The so called "Non-uniform Timoshenko beam model" employing Finite Element Method (FEM) was used to model structural part, while the hydrodynamic part was modelled by the classical 3D Boundary Integral Equation (BIE) technique. Modal approach was used to couple the two parts whereby the final structural deflection was split into a number of the structural 'dry' modes. The hydroelastic response of a barge to regular waves by employing 3D hydroelasticity was presented by Chen et al. [25] and findings were compared with experimental results.

Leibowitz [26] and Juncher [27] demonstrated the use of beam models for idealised ships analysis and hull vibrations at lower natural frequencies. Considering them as thin walled beams, the cross-section warping was considered using the St. Venant torsion theory by Kawai [28] and using Vlasov thin-walled beam theory [29]. In [30] and [31] classical beam girder theories with some improvements to account for discontinuous cross-sections were used, but lacked satisfactory results for open-sectioned beams and results for higher vibration modes. Advanced theories have been implemented in beam girder idealization of ships in several papers by Senjanovic and his co-workes, see for example [32, 33, 34, 35, 36, 37, 38]. These works pertain to the fact that many ship structures have large deck openings (such as container ships) making them resemble like open-section girders whose shear centers lie outside of cross-section. For example, in the paper by Senjanovic and Fan [32] a higher-order theory was developed with mode-dependent beam parameters. In Ref. [37] the effect of shear on torsion apart from its known influence on bending was also introduced. This work also included dry hull vibration analysis using 1D FEM for very large container ships and serves a commendable reference on refined beam models. In the same work, the results were correlated with 3D FEM results but only for some lower modes. In another paper, Senjanovic et al. [38] coupled horizontal flexural and torsional vibration of container ships were considered and discussed by idealizing them as ship-like girders.

The present paper proposes a novel refined 1D model based on the Carrera Unified Formulation (CUF) [39, 40] for the static and free vibration analyses of ship structures. According to CUF, beam theories with higher-order kinematics can be automatically developed by expressing the 3D displacement field as an arbitrary expansion of generic cross-sectional functions. Various classes of beam models can be formulated depending on the choice of these cross-sectional functions. For example, the Taylor Expansion (TE) class makes use of Taylor-like polynomials to enrich 1D kinematics and it has been validated in various papers in the literature for both static [41, 42] and free vibration analyses [43, 44, 45]. On the other hand, Lagrange polynomials are used to discretize the displacement field on the cross-section in LE (Lagrange Expansion) CUF beam models [46], and they are employed in this work to implement Component-Wise (CW) models [47, 48, 49, 50, 51] of marine structures.

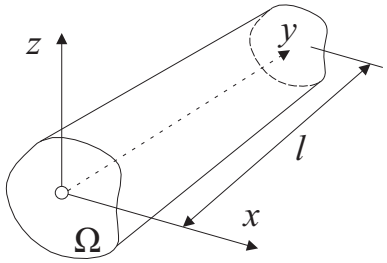

Figure 1: Generic beam model and related Cartesian reference system

2 Carrera Unified Formulation (CUF)

According to CUF, the generic 3D displacement field can be expressed in terms of a generic function F_τ:

$$\mathbf{u}(x,y,z) = F_\tau(x,z)\mathbf{u}_\tau(y), \qquad \tau = 1,2,....,M \tag{1}$$

where F_τ are the functions of the coordinates x and z over the cross-section (See Fig. 1); M is the number of expansion terms; $\mathbf{u}_\tau$ is the vector of the *generalized* displacements; and the repeated subscript, τ, indicates summation following the Einstein notation. In general, Eq. (1) describes the three-dimensional behavior of a structure and is an axiomatic model whose accuracy can be freely increased surpassing the limits of classic theories. The choice of cross-sections functions F_τ determines the class of the 1D CUF model adopted. In present work, Lagrange Expansion (LE) polynomials [52] have been used for expanding generalized beam unknowns. Using LE, we have only pure displacements as degrees of freedom (DoF). At a generic station along the beam length, an arbitrary shaped cross section is considered divided into *iso-parametric* Lagrange elements that may be 3-noded (L3), 4-noded (L4) or 9-noded (L9). The interpolation functions in the case of an L9 element are, for example,

$$\begin{aligned}
F_\tau &= \frac{1}{4}(\alpha^2 + \alpha\alpha_\tau)(\beta^2 + \beta\beta_\tau), && \tau = 1,3,5,7 \\
F_\tau &= \frac{1}{2}{\beta_\tau}^2(\beta^2 + \beta\beta_\tau)(1-\alpha^2) + \frac{1}{2}{\alpha_\tau}^2(\alpha^2 + \alpha\alpha_\tau)(1-\beta^2), && \tau = 2,4,6,8 \\
F_\tau &= (1-\alpha^2)(1-\beta^2), && \tau = 9
\end{aligned} \tag{2}$$

where α and β vary from -1 to +1, whereas α_τ and β_τ are the coordinates of the nine points whose numbering and location in the natural coordinate frame are shown in Fig. 2.

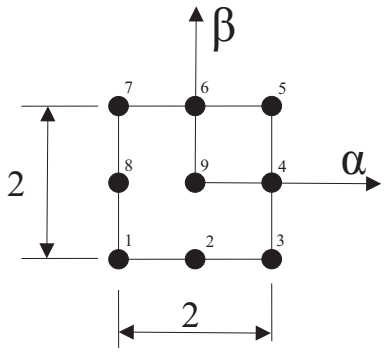

Figure 2: L9 element in natural coordinates

3 Finite Element Formulation

3.1 *Preliminaries*

The present beam model involves the coordinate system as shown in Fig. 1. The beam length is from 0 to l and the cross section is Ω. The stress $\boldsymbol{\sigma}$ and strain $\boldsymbol{\epsilon}$ vectors may be written as follows:

$$\boldsymbol{\sigma} = \left\{ \begin{array}{cccccc} \sigma_{yy} & \sigma_{xx} & \sigma_{zz} & \sigma_{xz} & \sigma_{yz} & \sigma_{xy} \end{array} \right\}^T, \boldsymbol{\epsilon} = \left\{ \begin{array}{cccccc} \epsilon_{yy} & \epsilon_{xx} & \epsilon_{zz} & \epsilon_{xz} & \epsilon_{yz} & \epsilon_{xy} \end{array} \right\}^T \tag{3}$$

Considering small displacements, the linear strain-displacement relation is given as:

$$\boldsymbol{\epsilon} = \mathbf{D}\mathbf{u} \tag{4}$$

where $\mathbf{D}$ is the linear differential operator on $\mathbf{u}$ and it is given as follows:

$$\mathbf{D} = \begin{bmatrix} 0 & \frac{\partial}{\partial y} & 0 \\ \frac{\partial}{\partial x} & 0 & 0 \\ 0 & 0 & \frac{\partial}{\partial z} \\ \frac{\partial}{\partial z} & 0 & \frac{\partial}{\partial x} \\ 0 & \frac{\partial}{\partial z} & \frac{\partial}{\partial y} \\ \frac{\partial}{\partial y} & \frac{\partial}{\partial x} & 0 \end{bmatrix} \tag{5}$$

The stress is related to strain through the constitutive law as follows:

$$\boldsymbol{\sigma} = \tilde{\mathbf{C}}\boldsymbol{\epsilon} \tag{6}$$

where $\tilde{\mathbf{C}}$ is the elastic stiffness matrix that, for an isotropic material, is

$$\tilde{\mathbf{C}} = \begin{bmatrix} \tilde{C}_{33} & \tilde{C}_{23} & \tilde{C}_{13} & 0 & 0 & 0 \\ \tilde{C}_{23} & \tilde{C}_{22} & \tilde{C}_{12} & 0 & 0 & 0 \\ \tilde{C}_{13} & \tilde{C}_{12} & \tilde{C}_{11} & 0 & 0 & 0 \\ 0 & 0 & 0 & \tilde{C}_{44} & 0 & 0 \\ 0 & 0 & 0 & 0 & \tilde{C}_{44} & 0 \\ 0 & 0 & 0 & 0 & 0 & \tilde{C}_{44} \end{bmatrix} \tag{7}$$

The expressions of the terms $\tilde{C}_{ij}$ and their dependency on elastic modulus, E, and Poisson ratio, ν, are available in [53].

3.2 *Fundamental Nuclei*

The beam is discretised along the length (y axis) to obtain finite elements. Following a typical FE procedure and by coupling with CUF (Eq. (1)), we can express the 3D displacement field as

$$\mathbf{u}(x, y, z) = F_\tau(x, z) N_i(y) \mathbf{q}_{\tau i} \tag{8}$$

where

$$\mathbf{q}_{\tau i} = \left\{ \begin{array}{ccc} q_{x_{\tau i}} & q_{y_{\tau i}} & q_{z_{\tau i}} \end{array} \right\}^T \tag{9}$$

is the 1D nodal unknown vector and N_i is the i-th shape function. The 1D shape functions are not reported here for the sake of brevity and can be found in [52]. The choice of the cross-section discretization for the LE class, is completely independent of the choice of the beam finite element to be used along the axis of the beam. Beam elements with four nodes (B4) were adopted in this work, which have cubic approximation along y-axis.

The governing equations in terms of FE matrices can be easily obtained by exploiting the weak form of the principle of virtual displacements. In the general case in which internal forces are equilibrated by external and inertial forces, we have

$$\delta L_{\text{int}} = \delta L_{\text{ext}} - \delta L_{\text{ine}} \tag{10}$$

where $L_{\text{int}} = \int_V \delta\boldsymbol{\epsilon}^T \boldsymbol{\sigma} \mathrm{d}V$ stands for the internal strain energy; L_{ine} is the work done by the external forces; and L_{ine} is the work of the inertial loading. δ stands for the usual virtual variation.

The virtual variation of the strain energy is rewritten hereinafter by using Eqs. (4), (6) and (8) as:

$$\delta L_{\text{int}} = \delta \mathbf{q}_{\tau i}^T \, \mathbf{K}^{ij\tau s} \, \mathbf{q}_{sj} \tag{11}$$

where $\mathbf{K}^{ij\tau s}$ is the 3×3 stiffness matrix in compact form termed as *Fundamental Nucleus (FN)*. The nine components of the stiffness matrix nucleus in the case of isotropic material are provided below and they are referred to as $K_{rc}^{ij\tau s}$, where r is the row number ($r = 1, 2, 3$) and c is the column

number ($c = 1, 2, 3$).

$$
\begin{aligned}
K_{11}^{ij\tau s} &= (\lambda + 2G) \int_\Omega F_{\tau,x} F_{s,x} \mathrm{d}\Omega \int_l N_i N_j \mathrm{d}y + G \int_\Omega F_{\tau,z} F_{s,z} \mathrm{d}\Omega \int_l N_i N_j \mathrm{d}y + \\
&\quad G \int_\Omega F_\tau F_s \mathrm{d}\Omega \int_l N_{i,y} N_{j,y} \mathrm{d}y \\
K_{12}^{ij\tau s} &= \lambda \int_\Omega F_{\tau,x} F_s \mathrm{d}\Omega \int_l N_i N_{j,y} \mathrm{d}y + G \int_\Omega F_\tau F_{s,x} \mathrm{d}\Omega \int_l N_{i,y} N_j \mathrm{d}y \\
K_{13}^{ij\tau s} &= \lambda \int_\Omega F_{\tau,x} F_{s,z} \mathrm{d}\Omega \int_l N_i N_j \mathrm{d}y + G \int_\Omega F_{\tau,z} F_{s,x} \mathrm{d}\Omega \int_l N_i N_j \mathrm{d}y \\
K_{21}^{ij\tau s} &= \lambda \int_\Omega F_\tau F_{s,x} \mathrm{d}\Omega \int_l N_{i,y} N_j \mathrm{d}y + G \int_\Omega F_{\tau,x} F_s \mathrm{d}\Omega \int_l N_i N_{j,y} \mathrm{d}y \\
K_{22}^{ij\tau s} &= G \int_\Omega F_{\tau,z} F_{s,z} \mathrm{d}\Omega \int_l N_i N_j \mathrm{d}y + G \int_\Omega F_{\tau,x} F_{s,x} \mathrm{d}\Omega \int_l N_i N_j \mathrm{d}y + \\
&\quad (\lambda + 2G) \int_\Omega F_\tau F_s \mathrm{d}\Omega \int_l N_{i,y} N_{j,y} \mathrm{d}y \\
K_{23}^{ij\tau s} &= \lambda \int_\Omega F_\tau F_{s,z} \mathrm{d}\Omega \int_l N_{i,y} N_j \mathrm{d}y + G \int_\Omega F_{\tau,z} F_s \mathrm{d}\Omega \int_l N_i N_{j,y} \mathrm{d}y \\
K_{31}^{ij\tau s} &= \lambda \int_\Omega F_{\tau,z} F_{s,x} \mathrm{d}\Omega \int_l N_i N_j \mathrm{d}y + G \int_\Omega F_{\tau,x} F_{s,z} \mathrm{d}\Omega \int_l N_i N_j \mathrm{d}y \\
K_{32}^{ij\tau s} &= \lambda \int_\Omega F_{\tau,z} F_s \mathrm{d}\Omega \int_l N_i N_{j,y} \mathrm{d}y + G \int_\Omega F_\tau F_{s,z} \mathrm{d}\Omega \int_l N_{i,y} N_j \mathrm{d}y \\
K_{33}^{ij\tau s} &= (\lambda + 2G) \int_\Omega F_{\tau,z} F_{s,z} \mathrm{d}\Omega \int_l N_i N_j \mathrm{d}y + G \int_\Omega F_{\tau,x} F_{s,x} \mathrm{d}\Omega \int_l N_i N_j \mathrm{d}y + \\
&\quad G \int_\Omega F_\tau F_s \mathrm{d}\Omega \int_l N_{i,y} N_{j,y} \mathrm{d}y
\end{aligned}
\tag{12}
$$

where the comma denotes derivative; and G and λ are the Lamé's parameters. If Poisson ν and Young E moduli are used, one has $G = \frac{E}{(2(1+\nu)}$ and $\lambda = \frac{\nu E}{(1+\nu)(1-2\nu)}$. The strength of CUF is that the elemental stiffness matrix of any-order and class 1D structural model can be straightforwardly obtained by expanding the fundamental nucleus according to the summation indexes τ, s, i, and j. In fact, the formal expression of the components of the fundamental nucleus do not depend on the

type and order of F_τ functions.

In the present work, for the sake of brevity, the fundamental nuclei of the mass matrix and the loading vector are not reported. However, they can be found in [39], where detailed derivations and more details about CUF and related FE applications can be found.

4 Numerical Results

This section presents the effectiveness of using CUF beam models in structural analysis of practical ship structures involving geometric complexities. Beginning with simple idealization and validation as a beam for a destroyer ship from Ref. [9], CUF beam model is subsequently used to analyse more complex geometries such as stiffened-box and boat-like structures. The objective is to obtain the refined displacement kinematics as an initial approach towards analysis of more complex geometries such as container ships. In engineering practice, typical naval structures are complex and their FE model consist of employing 1D beams, 2D shells and 3D solid elements with fictitious links introduced to account for difference of kinematics at mutual interface locations of the three element types. With the present refined 1D models, all structural features such as beams, bulkheads, floors and hulls can be modelled with the same 1D CUF structural elements with various cross-sections each associated to each feature being modelled.

4.1 Destroyer Hull

An example of destroyer hull was addressed in Ref. [9], whereby the ship was modelled as a non-uniform beam. The available ship data has been used in the analysis using CUF beam model for the vibration analysis and results are compared for validation. Referring to Fig. 3, the destroyer ship is divided into 20 sections of equal length, each one modelled as a component for the present LE1D model. The data for each section is given in Table 1. Cross-section for each section has been idealised as a rectangle of height $h(y)$ and breadth $b(y)$. The results of the present model and ANSYS are shown in Table 2 and a good comparison is evident validating the effectiveness of LE beam model for structural analysis of practical ships.

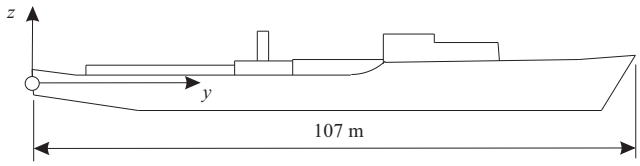

Figure 3: Destroyer ship geometry

Section ID	**Mass/Length (ton/m)**	$\mathbf{I}_{xx}$ (m^4)	**A** (m^2)	**Section ID**	**Mass/Length (ton/m)**	$\mathbf{I}_{xx}$ (m^4)	**A** (m^2)
1	10.21	0.68	0.044	11	26.56	4.33	0.089
2	10.81	1.20	0.054	12	28.77	4.26	0.088
3	13.58	1.79	0.064	13	23.48	4.26	0.086
4	43.17	2.50	0.072	14	46.25	4.25	0.077
5	39.88	3.34	0.079	15	39.07	4.08	0.070
6	26.06	3.76	0.085	16	15.40	3.71	0.069
7	25.04	4.04	0.089	17	12.11	3.24	0.070
8	25.26	4.30	0.090	18	10.90	2.74	0.071
9	35.90	4.38	0.089	19	6.75	2.24	0.072
10	27.01	4.38	0.089	20	1.18	2.10	0.071

Table 1: Input data for destroyer shown in Fig. 3

For the destroyer model, 20 sections of rectangular cross sections satisfy the area moment, I, and shear area, A, from Ref. [9]. The resulting configuration of the beam is such that almost all cross sections have lateral dimension (lying along x axis) considerably small compared to the vertical one (lying along z plane). Thus, the lowest modes predicted by present beam model are dominated by bending in lateral plane and are not reported. It may be noted that the results of Ref. [9] employ effects of various corrections applied onto the classic beam models whereas the LE model requires no such corrections.

For the complex structure of destroyer ship, available data from Ref. [9] is sufficient while attempting to employ classic beam theories. As a result, only the vertical bending frequencies are obtained in a dynamic analysis. Employing the present CUF LE model has satisfactorily provided results close to the published beam results but the capacity of present model is much higher to encompass various other deformed configurations such as cross-section warpage associated with torsional modes in a practical ship. This capability of the CUF model will demonstrated in the subsequent sections.

Mode	LE Beam (Hz)	Ref [9] (Hz)	ANSYS Beam (Hz)
1	1.97	2.16	2.22
2	3.97	4.33	4.64
3	6.13	6.37	5.04
4	8.94	9.24	8.28
5	11.63	11.8	12
6	13.56	13.76	13.32

Table 2: Natural vibration frequencies in vertical bending for destroyer of Fig. 3

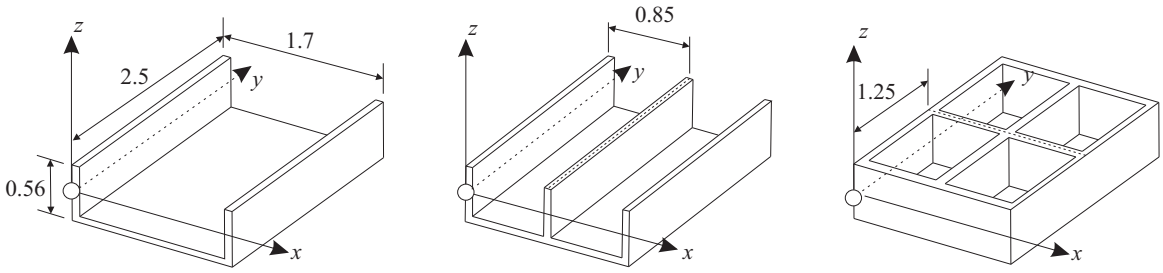

(a) Box with 2 walls

(b) Box with 2 walls and 1 stiffener

(c) Box with 4 walls and 2 crossing stiffeners

Figure 4: Box-like structure geometries (dimensions in meters)

4.2 Box-like structures

4.2.1 Modal analysis

The free vibration analysis of a box-like structure is presented for the three configurations as shown in Fig. 4. The boundary conditions for this analysis are free-free and the material is an aluminum alloy with the following characteristics: $E = 75$ GPa, $\nu = 0.33$, and material density $\rho = 2700$ Kg/m3. The wall thicknesses at all places is 10 mm. With the same overall dimensions, the simple configuration, Fig. 4 (a), is stiffened by introducing inner walls thereby complicating the problem as shown in Fig. 4 (b) and (c).

As an example, the next Fig. 5 clarify the three FE approaches employed for the analysis of configuration of Fig. 4 (c). The shell surfaces shown in Fig. 5 (a) are the mid-planes of the shell elements (ANSYS Shell-281) and each node has 6 DoF. The solid element mesh Fig. 5 (b) is made up of ANSYS Solid-186 elements with 3 DoF at each node. For the CUF Beam model Fig. 5 (c), beam elements are aligned along y-axis and cross-sections lie in x-z planes. The beam is discretized

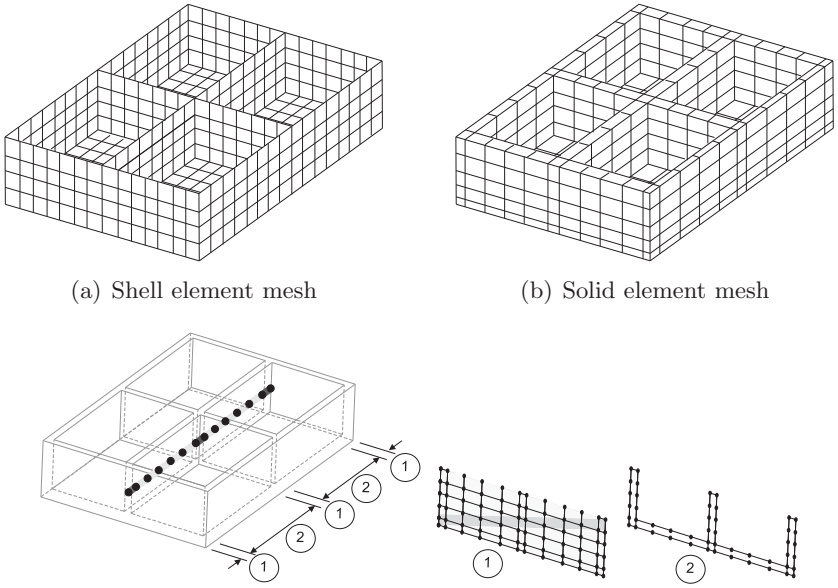

(a) Shell element mesh

(b) Solid element mesh

(c) CUF LE Beam elements mesh with two cross section types

Figure 5: Various FE approaches to model the box-like structure of Fig. 4 (c)

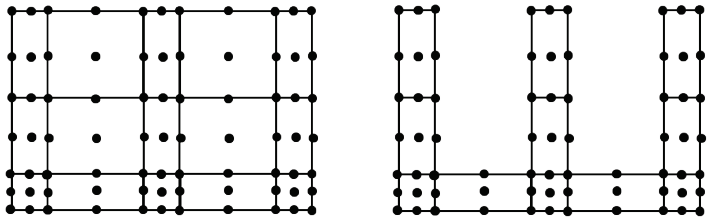

(a) L9 Mesh for Cross section-1

(b) L9 Mesh for Cross section-2

Figure 6: Cross section mesh

into 13 elements along y-axis. There are two types of cross-sections encircled as 1 and 2. Each cross-section type consists of Lagrange L9 elements and each L9 node has 3 DoF. For illustrative purposes, Fig. 6 shows an example of LE discretization for the two cross-sections of the structure in Fig. 5 (c). The cross section mesh of Fig. 6 (a) is referred to as 15L9 and the one in Fig.6 (b) as 11L9 indicating 15 and 11 9-noded Lagrange elements are employed in each mesh respectively.

Natural frequencies obtained from the analysis of free-free box of Fig. 4 (a) to (c) are presented in Tables 3 to 5 and the corresponding first and fourth mode shapes are shown in Fig. 7. The results from the ANSYS models come from convergence analyses.

A comparison between the aforementioned three approaches for the all three configurations of Fig.

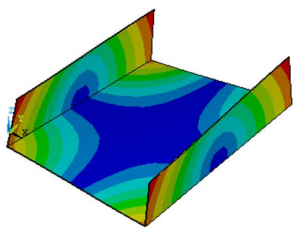

(a) Config. Fig. 4 (a) Mode 1: ANSYS

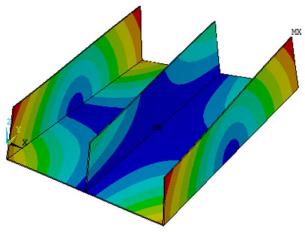

(b) Config. Fig. 4 (b) Mode 1: ANSYS

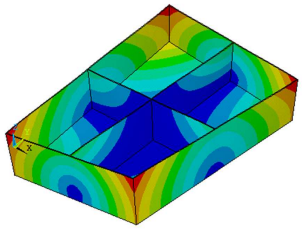

(c) Config. Fig. 4 (c) Mode 1: ANSYS

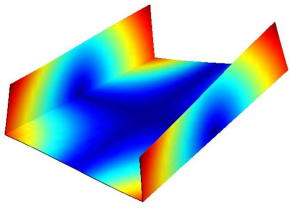

(d) Config. Fig. 4 (a) Mode 1: LE CUF Model

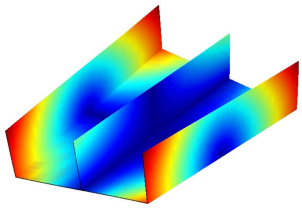

(e) Config. Fig. 4 (b) Mode 1: LE CUF Model

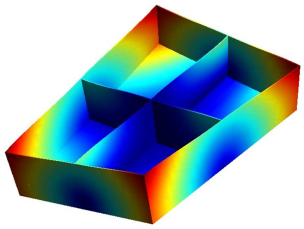

(f) Config. Fig. 4 (c) Mode 1: LE CUF Model

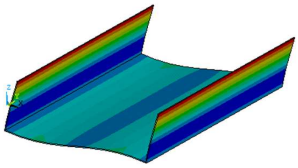

(g) Config. Fig. 4 (a) Mode 4: ANSYS

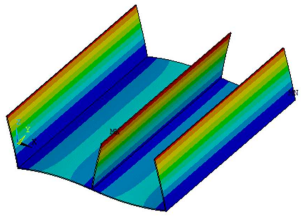

(h) Config. Fig. 4 (b) Mode 4: ANSYS

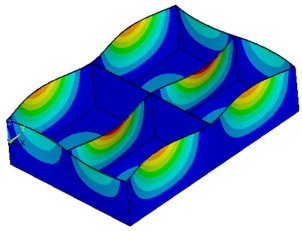

(i) Config. Fig. 4 (c) Mode 4: ANSYS

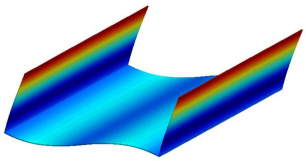

(j) Config. Fig. 4 (a) Mode 4: LE CUF Model

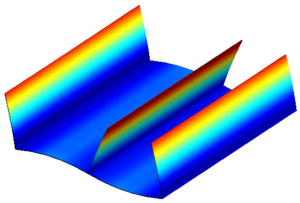

(k) Config. Fig. 4 (b) Mode 4: LE CUF Model

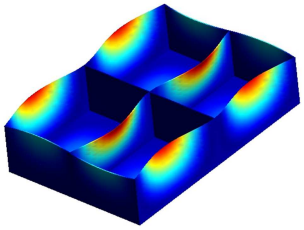

(l) Config. Fig. 4 (c) Mode 4: LE CUF Model

Figure 7: First and forth mode shapes for the box-like configurations of Fig. 4(a), (b) and (c)

(DOFs)	5L9 Model (1023)	8L9 Model (4743)	12L9 Model (6975)	ANS2D (51678)	ANS3D (153948)
Mode 1	6.52	5.26	5.23	5.16	5.22
Mode 2	9.79	8.41	8.25	8.04	8.11
Mode 3	19.30	14.21	14.00	13.73	13.89
Mode 4	28.30	19.57	18.39	17.41	17.65
Mode 5	48.10	22.73	21.91	21.11	21.41
Mode 6	49.30	23.01	22.01	21.48	21.72
Mode 7	50.60	32.87	29.30	26.05	26.44
Mode 8	53.90	38.79	31.61	28.44	28.87
Mode 9	69.50	46.15	31.93	30.97	31.43
Mode 10	71.00	48.09	37.76	35.07	35.62

Table 3: Natural frequencies (Hz) for the free-free box-like case of Fig. 4 (a)

(DOFs)	16L9 Model (6975)	ANS2D (61710)	ANS3D (73824)
Mode 1	5.65	5.54	5.61
Mode 2	7.75	7.50	7.59
Mode 3	12.61	12.23	12.39
Mode 4	15.03	14.49	14.70
Mode 5	19.73	19.16	19.44
Mode 6	25.84	22.80	23.21
Mode 7	27.77	24.92	25.36
Mode 8	29.21	26.43	27.01
Mode 9	31.19	28.68	29.26
Mode 10	31.30	30.46	30.91

Table 4: Natural Frequencies (Hz) for free-free box-like case of Fig. 4 (b)

(DOFs)	15L9 Model (8352)	20L9 Model (10872)	28L9 Model (14364)	ANS2D (81114)	ANS3D (99366)	ANS3D (238200)
Mode 1	8.60	8.48	7.47	7.10	7.19	7.19
Mode 2	40.29	39.88	39.66	37.95	38.69	38.52
Mode 3	44.51	44.19	41.89	39.01	39.78	39.61
Mode 4	55.90	55.011	44.15	42.70	43.44	43.28
Mode 5	56.10	55.21	46.02	43.53	44.28	44.12
Mode 6	58.86	57.95	49.29	45.71	46.66	46.47
Mode 7	61.90	61.04	55.20	52.11	53.08	52.88
Mode 8	76.03	74.88	74.43	62.84	64.05	63.83
Mode 9	79.81	78.77	78.09	64.21	65.42	65.23
Mode 10	88.84	87.51	86.15	68.32	69.58	69.37

Table 5: Natural Frequencies (Hz) for free-free box-like case of Fig. 4 (c)

4 (a) to (c) clearly shows that reduced DoF are required for converged LE 1D beam model compared to the solid (ANS3D) and shell (ANS2D) models for the same level of accuracy. Lowest deformed modes were torsional ones involving cross sectional warping that have been captured by CUF beam model which otherwise was possible only through costly ANS2D or ANS3D models. Modes such as forth one for the configuration shown in Fig.4 (a) and (b) involve in-plane displacement along the cross-section that has been satisfactorily captured through CUF beam model, ANS2D and ANS3D and was not possible through classic beam theories. As a result of adding walls, the increase in stiffness of the structure is evident through the increase in natural frequencies. Also, as a result of adding walls, various global modes are no more present and, resultantly, the local modes are lower modes, thanks to the detailed kinematic capturing capability of CUF beam model.

4.2.2 Static analysis

Static analyses of the box structure shown in Fig. 4 (c) were performed by considering different loading and boundary conditions, as shown in Fig. 8 (a) to (d). In Fig. 8 (a) and (b) a point load is applied in the middle of the stiffening members, and boundary conditions applied to the four edges of the bottom face are SFSF (S=Simply-supported and F=Free-Free) and SSSS, respectively. Similarly, in Fig. 8 (c) and (d), the loading is a Uniformly Distributed Load (UDL) with boundary conditions respectively being SFSF and SSSS.

The results for each case, deflections and stresses, are presented in Tables 6 to 7, whereas the deflected shapes, as obtained from ANS3D and the present LE beam model, are shown in Fig.10 to 13 for the respective cases. Fig.9 (b) shows the selected locations (A to H) on the surface at $z = -0.275$ m (midway through the thickness) for obtaining the displacements and the directional stresses. Taking into account the symmetry in the structure, only the results at points A and E are being reported here.

From the results of the static analysis of box-like configuration of Fig. 8 (a), it can be inferred that the required DoF are significantly reduced for LE 1D beam model compared to the solid (ANS3D) model for a comparable level of accuracy. Using LE beam models, loads and boundary conditions can be applied at any point in 3D space of the structure. The realistic deformation of the structure is captured throughout the geometry involving out-of-plane displacements for cross

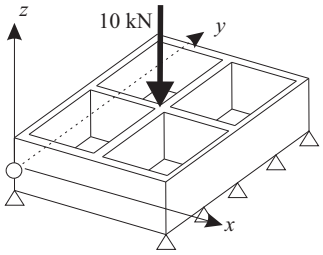

(a) Point Load with SFSF Boundary Condition

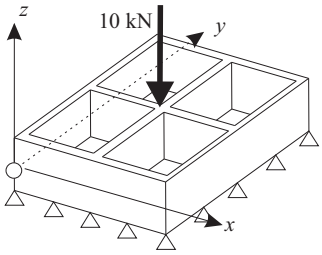

(b) Point Load with SSSS Boundary Condition

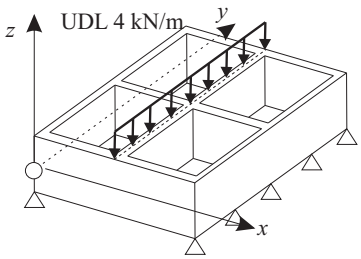

(c) Uniformly Distributed Load with SFSF Boundary Condition

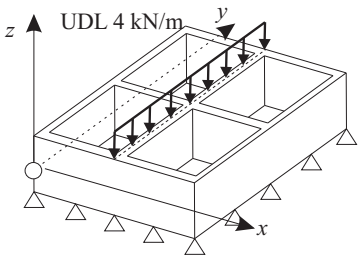

(d) Uniformly Distributed Load with SSSS Boundary Condition

Figure 8: Four cases of loading and boundary conditions

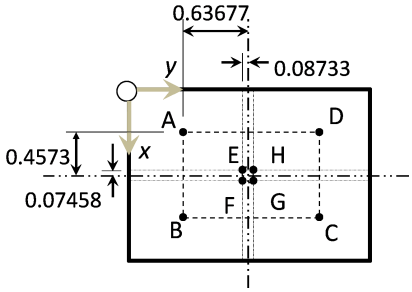

Figure 9: Plan view of the verification points for results

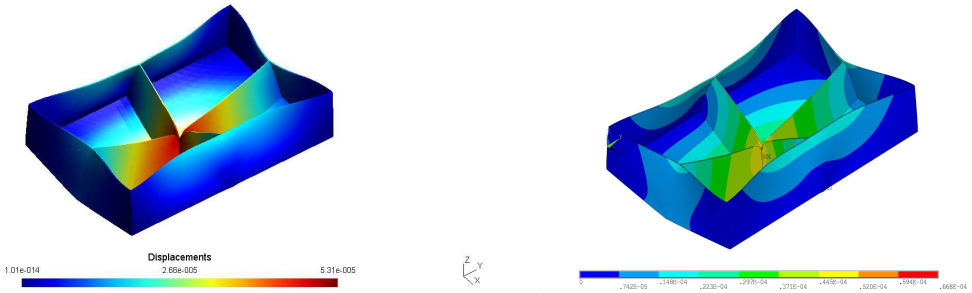

(a) Static Deflection from LE CUF Model

(b) Static Deflection from ANSYS

Figure 10: Deflected box under the loading shown in Fig. 8 (a)

Point	**Model (DOFs)**	**Displacements ($\times 10^{-6}$ m)**		
		u	v	w
A	CUF (27288)	0.289	-0.843	-18.576
	ANS3D (515103)	0.294	-0.857	-18.776
E	CUF (27288)	-0.336	-0.088	-42.476
	ANS3D (515103)	-0.334	-0.090	-42.997

Point	**Model (DOFs)**	**Stresses ($\times 10^5$ Pa)**					
		$\boldsymbol{\sigma}_{xx}$	$\boldsymbol{\sigma}_{yy}$	$\boldsymbol{\sigma}_{zz}$	$\boldsymbol{\sigma}_{xy}$	$\boldsymbol{\sigma}_{xz}$	$\boldsymbol{\sigma}_{yz}$
A	CUF (27288)	0.130	0.726	0.004	-0.543	-0.007	-0.009
	ANS3D (515103)	0.122	0.744	0.000	-0.549	-0.003	-0.002
E	CUF (27288)	4.058	2.892	-0.028	-1.049	-0.637	0.052
	ANS3D (515103)	4.278	2.919	-0.008	-1.038	0.017	-0.018

Table 6: Results under the loading shown in Fig.8 (a); CUF and ANS3D refer to 77/29L9 and ANSYS Soild Models respectively.

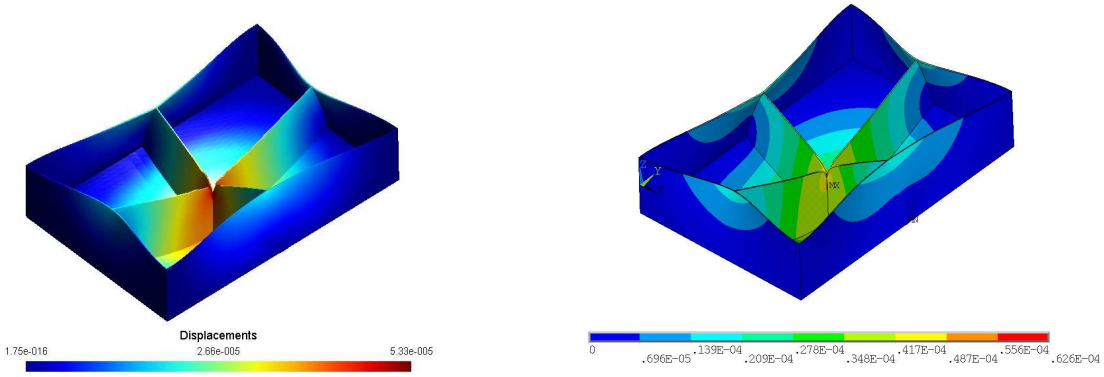

(a) Static Deflection from LE CUF Model

(b) Static Deflection from ANSYS

Figure 11: Deflected box under the loading shown in Fig. 8 (b)

Point	**Model (DOFs)**	**Displacements ($\times 10^{-6}$ m)**		
		u	v	w
A	CUF (27288)	0.063	-0.2382	-13.017
	ANS3D (515103)	0.067	-0.248	-13.120
E	CUF (27288)	-0.302	-0.048	-38.350
	ANS3D (515103)	-0.300	-0.049	-38.849

Point	**Model (DOFs)**	**Stresses ($\times 10^5$ Pa)**					
		$\boldsymbol{\sigma}_{xx}$	$\boldsymbol{\sigma}_{yy}$	$\boldsymbol{\sigma}_{zz}$	$\boldsymbol{\sigma}_{xy}$	$\boldsymbol{\sigma}_{xz}$	$\boldsymbol{\sigma}_{yz}$
A	CUF (27288)	-0.078	-0.067	0.002	-0.089	-0.011	-0.016
	ANS3D (515103)	-0.073	-0.051	0.000	-0.103	-0.004	-0.002
E	CUF (27288)	3.618	2.290	-0.024	-1.049	-0.503	0.046
	ANS3D (515103)	3.843	2.329	-0.007	-1.021	0.005	-0.013

Table 7: Results under the loading shown in Fig. 8 (b); CUF and ANS3D refer to 77/29L9 and ANSYS Soild Models respectively.

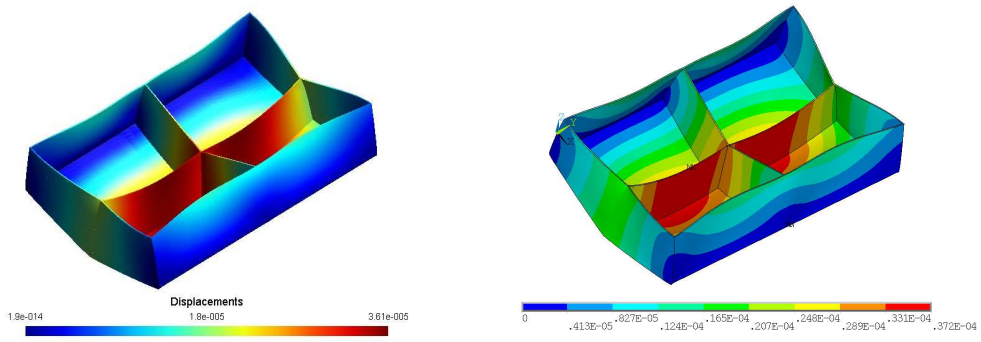

(a) Static Deflection from LE CUF Model

(b) Static Deflection from ANSYS

Figure 12: Deflected box under static point load of Fig. 8 (c)

Point	Model (DOFs)	Displacements ($\times 10^{-6}$ m)		
		u	v	w
A	CUF (27288)	0.318	-0.587	-18.642
	ANS3D (515103)	0.335	-0.593	-19.047
E	CUF (27288)	-0.356	0.217	-31.703
	ANS3D (515103)	-0.362	0.234	-31.524

Point	Model (DOFs)	Stresses ($\times 10^5$ Pa)					
		σ_{xx}	σ_{yy}	σ_{zz}	σ_{xy}	σ_{xz}	σ_{yz}
A	CUF (27288)	0.268	0.628	0.000	-0.421	-0.005	-0.005
	ANS3D (515103)	0.281	0.654	0.000	-0.425	-0.004	-0.001
E	CUF (27288)	3.081	0.097	-0.034	-0.214	0.051	-1.078
	ANS3D (515103)	3.154	-0.152	-0.008	-0.268	-0.029	0.084

Table 8: Results under the loading shown in Fig. 8 (c); CUF and ANS3D refer to 77/29 L9 and ANSYS Soild Models respectively.

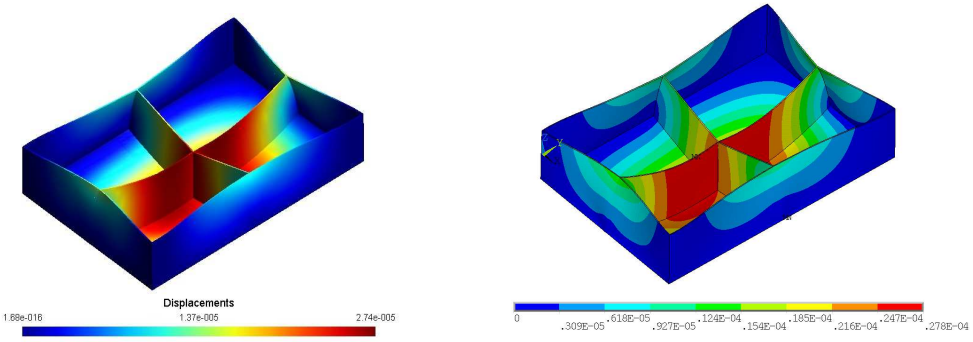

(a) Static Deflection from LE CUF Model

(b) Static Deflection from ANSYS

Figure 13: Deflected box under the loading shown in Fig. 8 (d)

Point	Model (DOFs)	Displacements ($\times 10^{-6}$ m)		
		u	v	w
A	CUF (27288)	0.094	-0.055	-11.460
	ANS3D (515103)	0.099	-0.037	-11.733
E	CUF (27288)	-0.284	0.201	-25.199
	ANS3D (515103)	-0.288	0.221	-24.817

Point	Model (DOFs)	Stresses ($\times 10^5$ Pa)					
		$\boldsymbol{\sigma}_{xx}$	$\boldsymbol{\sigma}_{yy}$	$\boldsymbol{\sigma}_{zz}$	$\boldsymbol{\sigma}_{xy}$	$\boldsymbol{\sigma}_{xz}$	$\boldsymbol{\sigma}_{yz}$
A	CUF (27288)	0.065	-0.082	-0.002	0.013	-0.010	-0.016
	ANS3D (515103)	0.082	-0.086	0.000	0.022	0.000	-0.004
E	CUF (27288)	2.405	-0.184	-0.028	-0.230	0.042	-0.862
	ANS3D (515103)	2.457	-0.440	-0.007	-0.256	-0.022	0.065

Table 9: Results under the loading shown in Fig. 8 (d); CUF and ANS3D refer to 77/29 L9 and ANSYS Soild Models respectively.

sections. Directional stresses calculated from the deformed configuration of LE beam model are comparable with those found from ANS3D. The localised deformation of point loading is realistically captured in Fig.10 and Fig.11 and that of UDL in Fig.12 and Fig.13. Increasing boundary condition application points, reduces vertical deflection and stresses and vice versa. The sharp increase in vertical deflection in case of point load is lessened compared to the case of UDL.

4.3 Boat-like structures

The usefulness of the present refined beam model is demonstrated through the free vibration analysis of the boat-like structure for which four configurations are shown in Fig. 14. The boundary conditions for this analysis are free-free and the material is the same aluminum as in the previous analysis cases. Figure 14 (a) is the simple hull with flat faces, then it is stiffened through a longeron in the middle (Fig. 14 (b)) and then further stiffened by introducing three transverse and two edge

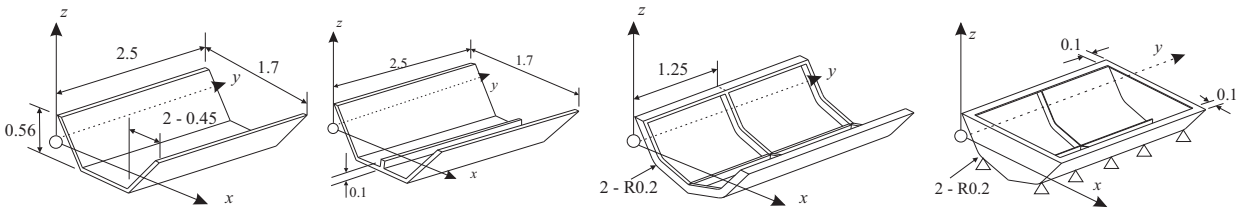

(a) Flat hull with no stiffeners (b) Flat hull with 1 stiffener (c) Flat hull with 2 crossing stiffeners (d) Flat hull with end walls

Figure 14: Boat-like structure geometries (dimensions in meters)

(DOFs)	**CUF 13L9 (7533)**	**CUF 19L9 (10881)**	**ANS2D (117126)**	**ANS2D (29766)**	**ANS3D (53910)**	**ANS3D (121695)**
Mode 1	6.47	6.46	6.37	6.37	6.45	6.45
Mode 2	9.98	9.88	9.65	9.65	9.84	9.83
Mode 3	14.48	14.40	14.13	14.13	14.35	14.34
Mode 4	24.23	24.11	23.71	23.71	23.99	23.98
Mode 5	26.42	26.10	25.46	25.46	25.83	25.81
Mode 6	27.52	27.09	26.19	26.19	26.73	26.70
Mode 7	30.81	30.43	29.56	29.56	30.10	30.07
Mode 8	40.16	39.97	39.42	39.41	39.76	39.75
Mode 9	42.26	41.83	41.05	41.05	41.44	41.42
Mode 10	61.55	60.63	58.51	58.51	59.39	59.37

Table 10: Comparison of natural frequencies of the boat-like structure of Fig. 14 (a)

stiffeners. The configuration in Fig. 14 (d) has four edge stiffeners and two end walls and has simply supported boundary conditions applied to edge fillets of R0.2. The width of each stiffener is 100 mm and thickness is 10 mm.

The natural frequencies obtained from the analysis of free-free boat of Fig. 14 (a) to (c) are presented in Tables 10 to 12 and the mode shapes for configuration of Fig. 14 (c) and (d) are shown in Figs. 15 and 16. A comparison between the aforementioned three approaches (CUF beam, shell and solid FEM models) for the all the configurations clearly show the reduced DoF required for converged LE 1D beam model compared to the solid and shell models for the same level of accuracy.

The results of the modal analysis of the boat-like configurations of Fig. 14 (a) to (d) show that for all the four configurations, there is a significant decrease in DoF compared to the corresponding ANSYS models. Similar to box-like configuration, the lower modes are torsional ones with LE beam model capturing cross-sectional warpage. Presence of stiffeners enhances the structural rigidity, which is evident through the increasing in natural frequencies. Localised vibration modes of the

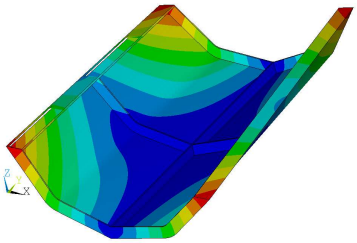

(a) Mode-1: ANSYS

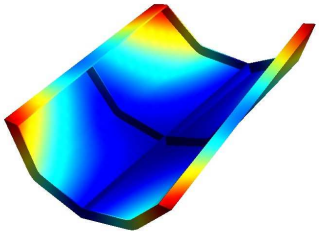

(b) Mode-1: 20/34L9 CUF Beam Model

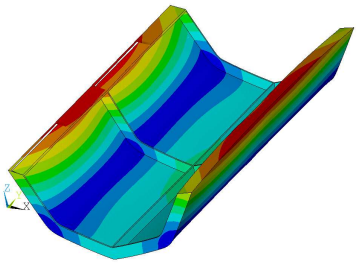

(c) Mode-2: ANSYS

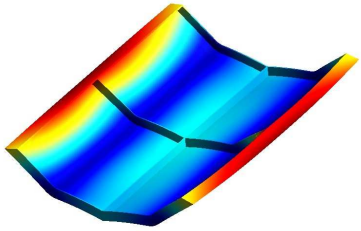

(d) Mode-2: 20/34L9 CUF Beam Model

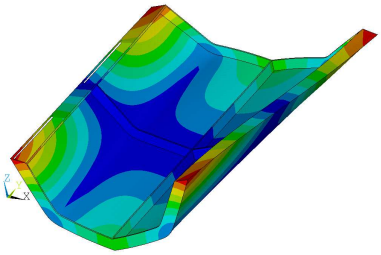

(e) Mode-3: ANSYS

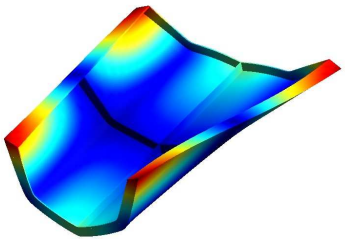

(f) Mode-13: 20/34L9 CUF Beam Model

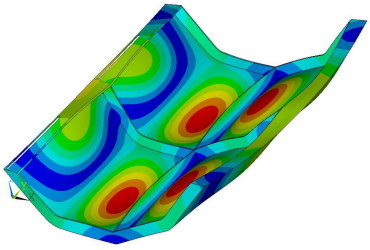

(g) Mode-3: ANSYS

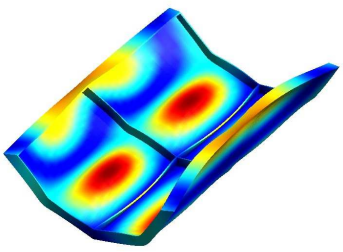

(h) Mode-4: 20/34L9 CUF Beam Model

Figure 15: Deformed modes 1 to 8 for configuration of Fig. 14 (c)

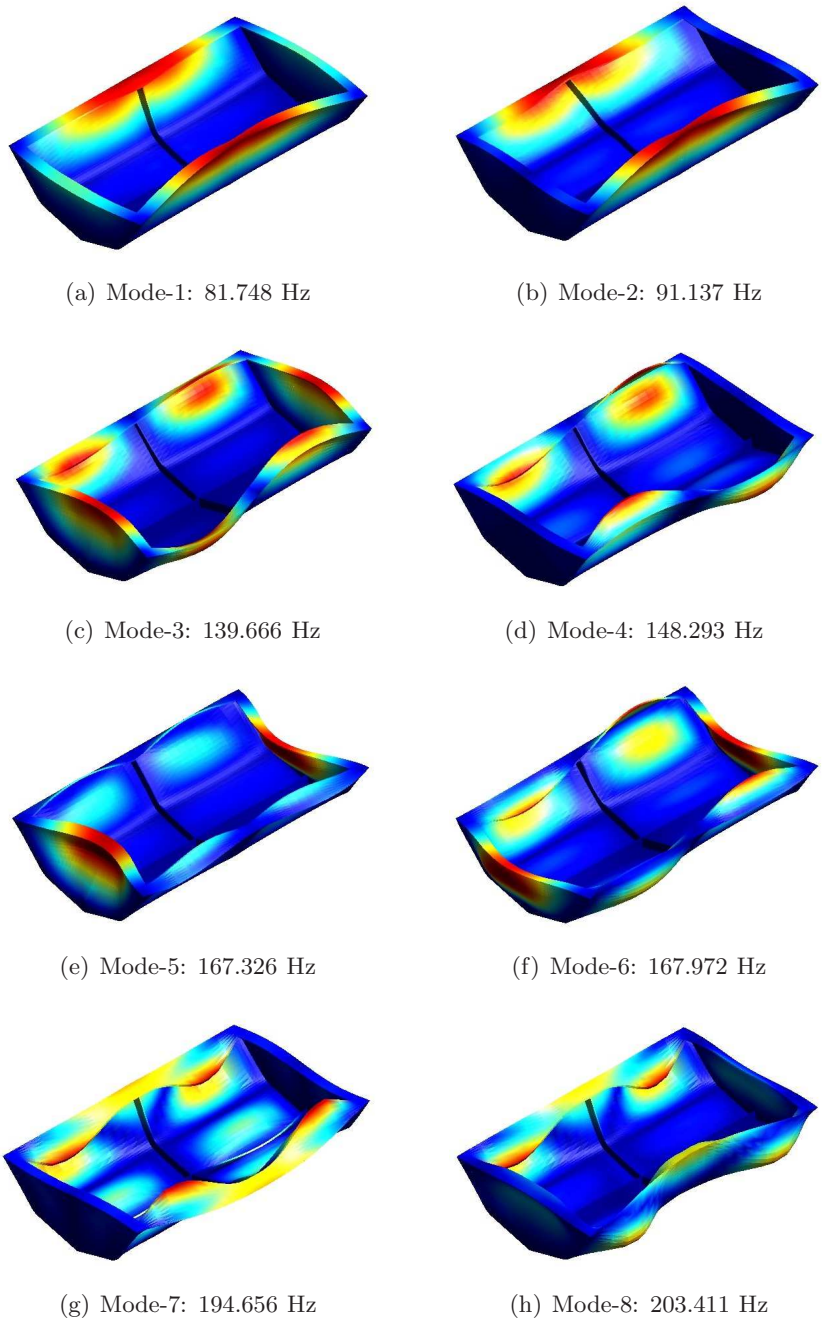

(a) Mode-1: 81.748 Hz

(b) Mode-2: 91.137 Hz

(c) Mode-3: 139.666 Hz

(d) Mode-4: 148.293 Hz

(e) Mode-5: 167.326 Hz

(f) Mode-6: 167.972 Hz

(g) Mode-7: 194.656 Hz

(h) Mode-8: 203.411 Hz

Figure 16: Deformed modes 1 to 8 for configuration of Fig. 14 (d)

(DOFs)	20L9 (11439)	ANS2D (32280)	ANS3D (63324)
1	6.66	6.54	6.62
2	9.81	9.54	9.73
3	14.29	13.98	14.19
4	25.76	25.24	25.43
5	26.10	25.42	25.75
6	26.79	25.91	26.34
7	30.29	29.38	29.84
8	41.54	40.69	41.00
9	41.88	41.06	41.39
10	58.96	55.96	57.15

Table 11: Comparison of natural frequencies of the boat-like structure of Fig. 14 (b)

(DOFs)	CUF 30L9 (11184)	CUF 54L9 (18672)	ANS2D (94302)	ANS2D (150270)	ANS3D (90702)	ANS3D (149637)
Mode 1	8.59	6.78	6.44	6.44	6.70	6.70
Mode 2	43.78	41.71	42.34	42.34	41.2	41.20
Mode 3	57.49	54.51	55.06	55.06	53.80	53.78
Mode 4	100.53	98.21	97.35	97.35	96.36	96.36
Mode 5	111.83	105.21	100.70	100.70	101.99	101.97
Mode 6	113.98	109.15	109.93	109.93	107.33	107.38
Mode 7	130.00	126.85	123.49	123.49	123.71	123.75
Mode 8	152.82	140.60	128.80	128.80	133.52	133.47
Mode 9	154.19	149.92	141.49	141.49	145.52	145.56
Mode 10	165.65	154.40	145.04	145.04	146.83	146.81

Table 12: Comparison of natural frequencies of the boat-like structure of Fig. 14 (c)

unsupported regions or edges replace the lower global vibration modes as a result of addition of stiffeners.

5 Conclusions

In this paper, a refined beam model with pure displacement variables and component-wise capabilities was presented to analyse complex ship structures and their idealizations. The efficacy of the present beam model was demonstrated for idealised ships, complex box-like and boat-like geometries by considering both modal and static analyses. The results in each case have been close to reference solutions from the literature and the 3D results of commercial software, ANSYS, with required DoF more than ten times lower. The CUF affords a possibility to capture detailed kinematics of beam

cross-section and the component-wise LE approach has enabled to captured all the structural features such as hulls, ribs, bulkheads and floors through the same 1D beam formulation at much lower computational cost compared to the 3D and 2D solutions.

References

[1] Euler L., De curvis elasticis, Lausanne and Geneva Bousquet, 1744.

[2] Timoshenko S.P., On the corrections for shear of the differential equation for transverse vibrations of prismatic bars, *Philosophical Magazine* 41, pp. 744746, 1922.

[3] Timoshenko S.P., On the transverse vibrations of bars of uniform crosssection, *Philosophical Magazine* 43, pp. 125131, 1922.

[4] John W.G., On the strength of iron ship, *Trans Inst Naval Arch* 15, pp. 7493, 1874

[5] Paik J.K., Thayamballi A.K., Pedersen P.T., Park Y.-II, Ultimate strength of ship hulls under torsion, *Ocean Engineering* 28, pp. 10971133, 2001.

[6] Yao T., Hull girder strength, *Marine Structures* 16, pp. 113, 2003.

[7] Bishop R.E.D., Price W. G., On modal analysis of ship strength, *Proceedings of The Royal Society A Mathematical Physical and Engineering Sciences* 341, pp. 121134, 1974

[8] Bishop R.E.D., Price W. G., Ship strength as a problem of structural dynamics, *The Naval Architect* 2, pp. 6163, 1975.

[9] Bishop R.E.D., Price W. G., *Hydroelasticity of Ships*, Cambridge University Press, 1979.

[10] Wu Y.S., *Hydroelasticity of floating bodies*, Brunel University, 1984.

[11] Price W.G., Wu Y.S., Hydroelasticity of marine structures, Sixteenth International Congress of Theoretical and Applied Mechanics (IUTAM), Lyngby, Denmark: Sectional Lecture, 1985, S10.

[12] Bishop R.E.D., Price W.G., Wu Y.S., A general linear hydroelasticity theory of floating structures moving in a seaway, *Philosophical Transactions A* 316, pp. 375426, 1986

[13] Wu Y.S., Price W.G., Advances in hydroelasticity of ships. *Aero-hydroelasticity developments and applications*, (Ed. Cui E.J.), Seismological Press, pp. 2137, 1993.

[14] Chen X.J., Wu Y.S., Cui W.C., Jensen J.J., Review of hydroelasticity theories for global response of marine structures, *Ocean Engineering*, 33(34), pp. 439457, 2006.

[15] Lundgren J., Price W.G., Wu Y.S., A hydroelastic investigation into the behavior of a floating 'dry' dock in waves, *Royal Institution of Naval Architects Transactions* 131, 1989.

[16] Fu Y.N., Price W.G., Temarel P., The 'dry and wet' towage of a jack-up in regular and irregular waves. *Transactions RINA* 129, pp. 149159, 1987.

[17] Ergin A., Price W.G., Randall R., Temarel P., Dynamic characteristics of a submerged, flexible cylinder vibrating in infinite water depths, *Journal of Ship Research* 36, pp. 154167, 1992

[18] Wang Z.J., Li R.P., Shu Z., A study on hydroelastic response of box-type very large floating structures, *China Ocean Engineering*, 15(3), pp. 345354, 2001.

[19] Phan T.S., Temarel P., Hydroelastic responses of pontoon and semi-submersible types of very large floating structure in regular head waves, Proceedings of the International Conference on *Offshore mechanics and arctic engineering OMAE* 2, pp. 753763, 2002.

[20] Li R.P., Shu Z., Wang Z.J., A study on the hydroelastic behavior of box-typed very large floating structure in waves, Proceedings of the Third Conference on *New ship and marine technology*, Kobe, Japan, 2002, pp. 4148.

[21] Fu S.X., Fan J., Chen X.J., Cui W.C., Analysis method for the mooring system for a flexible floating body, *Proceedings of Deep Water Mooring System: Concepts, Design, Analysis, and Materials, Offshore Technology Research Center (OTRC) and Coasts, Oceans, Ports and Rivers Institute (COPRI) of ASCE*, Houston, Texas, USA, 2003, pp. 142151.

[22] Price W. G., Wu Y. S., Structural responses of a SWATH of multi-hulled vessel travelling in waves, Proceedings of the International Conference on *SWATH ships and advanced multi-hulled vessels*, Royal Institution of Naval Architects, London, 1985.

[23] Keane A. J., Temarel P., Wu X.J., Wu, Y.S., Hydroelasticity of non-beamlike ships in waves, *The dynamics of ships*, The Royal Society of London, 1991.

[24] Malenica S., Molin B., Remy, F., Senjanovic I., Hydroelastic response of a barge to impulsive and non-impulsive wave loads, Proceedings of the Third International Conference on *Hydroelasticity in marine technology*, Oxford, UK, 2003, pp.107115.

[25] Chen X. J., Moan T., Fu S.X., Cui W.C., Hydroelastic analysis of flexible floating structures in regular waves, Proceedings of International Conference on *Mechanical engineering and mechanics* 1-2, pp. 973977, 2005.

[26] Leibowitz R.C., A Method for Prediction of Slamming Forces and Response of a Ship Hull, *David Taylor Model Basin Report*, 1961.

[27] Jensen J.J., Madsen H.F., A review of ship hull vibration: Part IV: Comparision of Beam Models, *Shock and Vibration Digest* 9(7), pp. 13-28, 1977.

[28] Kawai T., The application of finite element methods to ship structures, *Computers & Structures* 3, pp. 11751194, 1973.

[29] Vlasov V.Z., *Thin-Walled Elastic Beams*, Washington: National Science Foundation, 1961.

[30] Wu J.S., Ho C.S., Analysis of wave-induced horizontal and torsion coupled vibrations of a ship hull, *Journal of Ship Research*31(4), pp. 235-252, 1987.

[31] Pedersen P.T., Torsional response of container ships, *Journal of Ship Research*29, pp. 194-205, 1985.

[32] Senjanović I., Fan Y., A higher-order theory of thin-walled girders with application to ship structures, *Computers & Structures* 43(1), pp. 3152, 1992.

[33] Senjanović I., *Ship Vibrations. Part 2*, Textbook. Zagreb: University of Zagreb, 1990. (in Croatian).

[34] Senjanović I., Fan Y., A higher-order theory of thin-walled girders with application to ship structures, *Computers & Structures* 43(1), pp. 3152, 1992.

[35] Senjanović I., Fan Y., A finite element formulation of initial ship cross-section properties, *Brodogradnja* 41(1), pp. 2736, 1993.

[36] Senjanović I., Catipovic I, Tomasevic S. Coupled horizontal and torsional vibrations of ship-like girders, *Thin-Walled Structures* 45, pp. 10021021, 2007.

[37] Senjanović, I., Tomašević S., Vladimir N., An advanced theory of thin-walled girders with application to ship vibrations, *Marine Structures* 22(3)pp. 387-437, 2009.

[38] Senjanović I., Ćatipović I., Tomašević S., Coupled flexural and torsional vibrations of ship-like girders, *Thin-Walled Structures* 45(12), pp. 1002-1021, 2007.

[39] Carrera E., Cinefra M., Petrolo M., Zappino E., *Finite Element Analysis of Structures through Unified Formulation*, John Wiley & Sons, 2014.

[40] Carrera E., Giunta G., Petrolo M.. *Beam Structures: Classical and Advanced Theories*, John Wiley & Sons, 2011. DOI: 10.1002/9781119978565.

[41] Carrera E., Giunta G., Nali P., Petrolo M., Refined beam elements with arbitrary cross-section geometries, *Computers and Structures*88(5-6), pp. 283–293, 2010.

[42] Carrera E., Pagani A., Analysis of Reinforced and Thin-walled Structures by Multi-line Refined 1D/Beam Models, *International Journal of Mechanical Sciences*75, pp. 278–287, 2013. DOI: 10.1016/j.ijmecsci.2013.07.010.

[43] Petrolo M., Zappino E., Carrera E., Refined free vibration analysis of one-dimensional structures with compact and bridge-like cross-sections, *Thin-Walled Structures* 56, pp. 49–61, 2012. DOI: 10.1016/j.tws.2012.03.011.

[44] Carrera E., Petrolo M., Varello A., Advanced Beam Formulations for Free Vibration Analysis of Conventional and Joined Wings, *Journal of Aerospace Engineering*, 2(2), pp. 282–293, 2012. DOI: 10.1061/(ASCE)AS.1943-5525.0000130.

[45] Pagani A., Boscolo M., Banerjee J.R., Carrera E., Exact dynamic stiffness elements based on one-dimensional higher-order theories for free vibration analysis of solid and thin-walled structures, *Journal of Sound and Vibration* 332(23), pp. 6104–6127, 2013. DOI: 10.1016/j.jsv.2013.06.023.

[46] Carrera E., Petrolo M., Refined Beam Elements with only Displacement Variables and Plate/Shell Capabilities, *Meccanica* 47(3), pp. 537–556, 2012. DOI: 10.1007/s11012-011-9466-5.

[47] Carrera E., Pagani A., Petrolo M., Classical, Refined and Component-wise Theories for Static Analysis of Reinforced-Shell Wing Structures, *AIAA Journal* 51(5), pp. 1255–1268, 2013. DOI: 10.2514/1.J052331.

[48] Carrera E., Pagani A., Petrolo M., Component-wise Method Applied to Vibration of Wing Structures, *Journal of Applied Mechanics* 80(4), art.no. 041012, 2013. DOI: 10.1115/1.4007849.

[49] Carrera E., Pagani A., Free vibration analysis of civil engineering structures by component-wise models, *Journal of Sound and Vibration*, Vol. 333, pp. 4597–4620, 2013. DOI: 10.1016/j.jsv.2014.04.063.

[50] Carrera E., Pagani A., Petrolo M., Refined 1D Finite Elements for the Analysis of Secondary, Primary, and Complete Civil Engineering Structures, *Journal of Structural Engineering* 141, art.no. 04014123, 2015. DOI: 10.1061/(ASCE)ST.1943-541X.0001076.

[51] Carrera E., Petrolo M., Refined One-Dimensional Formulations for Laminated Structure Analysis, *AIAA Journal* 50(1), pp. 176–189, 2012. DOI: 10.2514/1.J051219.

[52] Oñate E., *Structural Analysis with the Finite Element Method:Linear Statics vol.1*, Springer,2009,

[53] Reddy J.N., Mechanics of Laminated Composite Plates: Theory and Analysis, *CRC Press, New York, USA*, 1997.